

DETECTION OF BROAD H α EMISSION LINES IN THE LATE-TIME SPECTRA OF A HYDROGEN-POOR SUPERLUMINOUS SUPERNOVA

LIN YAN¹, R. QUIMBY^{2,3}, E. OFEK⁴, A. GAL-YAM⁴, P. MAZZALI^{5,6}, D. PERLEY^{7,8}, P. M. VREESWIJK⁴, G. LELOUDAS^{4,8},
A. DE CIA⁴, F. MASCI¹, S. B. CENKO^{9,10}, Y. CAO¹¹, S. R. KULKARNI¹¹, P. E. NUGENT^{12,13}, UMAA D. REBBAPRAGADA¹⁴,
P. R. WOŹNIAK¹⁵, AND O. YARON⁴

¹ Infrared Processing and Analysis Center, California Institute of Technology, Pasadena, CA 91125, USA; lyan@ipac.caltech.edu

² Department of Astronomy, San Diego State University, San Diego, CA 92182, USA

³ Kavli IPMU (WPI), UTIAS, The University of Tokyo, Kashiwa, Chiba, 277-8583, Japan

⁴ Department of Particle Physics and Astrophysics, Faculty of Physics, The Weizmann Institute of Science, Rehovot 76100, Israel

⁵ Astrophysics Research Institute, Liverpool John Moores University, IC2, Liverpool Science Park, 146 Brownlow Hill, Liverpool L3 5RF, UK

⁶ Max-Planck-Institut für Astrophysik, Karl-Schwarzschild-Strasse 1, D-85748 Garching, Germany

⁷ Department of Astronomy, California Institute of Technology, Pasadena, CA 91125, USA

⁸ Dark Cosmology Centre, Niels Bohr Institute, University of Copenhagen, Juliane Maries Vej 30, DK-2100 Copenhagen, Denmark

⁹ Astrophysics Science Division, NASA Goddard Space Flight Center, Mail Code 661, Greenbelt, MD 20771, USA

¹⁰ Joint Space-Science Institute, University of Maryland, College Park, MD 20742, USA

¹¹ Astronomy Department, California Institute of Technology, Pasadena, CA 91125, USA

¹² Lawrence Berkeley National Laboratory, Berkeley, CA 94720, USA

¹³ Astronomy Department, University of California, Berkeley, 501 Campbell Hall, Berkeley, CA 94720, USA

¹⁴ Jet Propulsion Laboratory, California Institute of Technology, Pasadena, CA 91109, USA

¹⁵ Space and Remote Sensing, ISR-2, MS-B244 Los Alamos National Laboratory Los Alamos, NM 87545, USA

Received 2015 August 5; accepted 2015 October 13; published 2015 November 23

ABSTRACT

iPTF13ehe is a hydrogen-poor superluminous supernova (SLSN) at $z = 0.3434$, with a slow-evolving light curve and spectral features similar to SN2007bi. It rises in 83–148 days to reach a peak bolometric luminosity of $\sim 1.3 \times 10^{44} \text{ erg s}^{-1}$, then decays slowly at $0.015 \text{ mag day}^{-1}$. The measured ejecta velocity is $\sim 13,000 \text{ km s}^{-1}$. The inferred explosion characteristics, such as the ejecta mass ($70\text{--}220 M_{\odot}$), and the total radiative and kinetic energy ($E_{\text{rad}} \sim 10^{51} \text{ erg}$, $E_{\text{kin}} \sim 2 \times 10^{53} \text{ erg}$), are typical of slow-evolving H-poor SLSN events. However, the late-time spectrum taken at +251 days (rest, post-peak) reveals a Balmer H α emission feature with broad and narrow components, which has never been detected before among other H-poor SLSNe. The broad component has a velocity width of $\sim 4500 \text{ km s}^{-1}$ and a $\sim 300 \text{ km s}^{-1}$ blueward shift relative to the narrow component. We interpret this broad H α emission with a luminosity of $\sim 2 \times 10^{41} \text{ erg s}^{-1}$ as resulting from the interaction between the supernova ejecta and a discrete H-rich shell, located at a distance of $\sim 4 \times 10^{16} \text{ cm}$ from the explosion site. This interaction causes the rest-frame r -band LC to brighten at late times. The fact that the late-time spectra are not completely absorbed by the shock-ionized H-shell implies that its Thomson scattering optical depth is likely ≤ 1 , thus setting upper limits on the shell mass $\leq 30 M_{\odot}$. Of the existing models, a Pulsational Pair Instability supernova model can naturally explain the observed $30 M_{\odot}$ H-shell, ejected from a progenitor star with an initial mass of $(95\text{--}150) M_{\odot}$ about 40 years ago. We estimate that at least $\sim 15\%$ of all SLSNe-I may have late-time Balmer emission lines.

Key words: supernovae: general – supernovae: individual (iPTF13ehe, SN2007bi, PTF12dam)

1. INTRODUCTION

In the past decade, studies of superluminous supernovae (SLSNe; Gal-Yam 2012) have flourished because of the significant increase in the number of discoveries from the new generations of deeper and wider transient surveys, such as the Palomar Transient Factory (PTF; Law et al. 2009; Rau et al. 2009), the Panoramic Survey Telescope & Rapid Response System (Kaiser et al. 2002), and the Catalina Real-time Transient Survey (Drake et al. 2009). These sources attracted a great deal of interest because of (1) their unusually high peak luminosities, which were brighter than -20.5 mag (AB), and (2) their extremely broad light curves (LCs) with very slow rise and decay rates (e.g., Nicholl et al. 2015). These SLSNe are $\sim 5\text{--}100$ times more luminous than normal type Ia and core-collapse SNe. Both unique features suggested new explosion physics and special properties of the progenitor stars.

The known SLSNe can be classified into two broad categories according to their optical spectra (Gal-Yam 2012). The first category shows hydrogen features, and is called

SLSN-II. The extremely large energy output and the detection of hydrogen imply that the progenitor star must have had a massive, extended H-rich envelope or circumstellar medium (CSM) when it exploded (Smith et al. 2007; Chevalier & Irwin 2011). The second category is comprised of SLSNe without any hydrogen in their spectra (e.g., Quimby et al. 2011). It is thought that their progenitor stars have lost their hydrogen envelope long before the supernova went off. Within this hydrogen-poor category, a sub-class, SLSN-R, displays an LC that fades extremely slowly, and was proposed to be mostly powered by massive amounts of radioactive decay material. The archetypal SLSN-R is SN2007bi (Gal-Yam et al. 2009). Of all H-poor SLSNe, a small fraction are SLSN-R, and the majority of the events are classified as SLSNe-I. Because of the late-time spectral similarities to SNe Ic (Pastorello et al. 2010), in some papers this entire class is referred to as SLSN-Ic (e.g., Ingera et al. 2013; Nicholl et al. 2013).

Various scenarios have been proposed to explain the observed characteristics of these extremely energetic transient

events. For hydrogen-poor SLSNe, it is speculated (Gal-Yam et al. 2009) that SLSNe-R are pair instability supernovae (PISNe), as predicted theoretically in the late 1960s (Barkat et al. 1967; Rakavy & Shaviv 1967; Bond et al. 1984; Heger & Woosley 2002; Scannapieco et al. 2005). In this model, a progenitor star with $150 M_{\odot} \leq M \leq 260 M_{\odot}$ first loses its H envelope, and develops a massive oxygen core of $60\text{--}130 M_{\odot}$, which can reach well above 3×10^8 K (γ -ray photons). At such a high temperature, γ -ray photons start to produce electron-positron pairs. This triggers a dramatic loss of radiative pressure, followed by rapid contraction, which then ignites burning of the He/O core. This chain of events becomes a runaway thermonuclear explosion in only a few seconds. More importantly, the rapid burning and complete disruption of the core can also synthesize several M_{\odot} of radioactive ^{56}Ni , orders of magnitude more than typically seen in normal SNe. It is this massive amount of radioactive material that was proposed to power the emission from SLSNe-R. A competing model is the spin-down of a rapidly rotating, highly magnetic neutron star (Mazzali et al. 2006; Kasen & Bildsten 2010; Woosley 2010) that can release enough energy to power the prolonged SLSN LC. Some studies suggest all H-poor SLSNe can be explained by this model (Inserra et al. 2013; Nicholl et al. 2013). Finally, a third model is interaction powered (e.g., Gezari et al. 2009; Miller et al. 2009; Young et al. 2010; Chevalier & Irwin 2011; Quimby et al. 2011; Sorokina et al. 2015)—either the supernova ejecta interacting with a H-poor CSM, or a collision between two dense, H-poor shells previously expelled due to pulsational pair instability supernova (PPISN, Woosley et al. 2007), which arises in a progenitor star with a smaller initial mass of $95\text{--}150 M_{\odot}$. In this case, the He/O core is smaller, between 40 and $60 M_{\odot}$, which is massive enough to produce electron-positron pairs, but not massive enough to trigger a thermonuclear runaway explosion. PPISN models predict multiple episodes of instabilities, which can expel the outer H-layer, followed by additional H-poor CSM shells. After enough mass is lost, the star undergoes a Fe-core-collapse supernova explosion.

For SLSN-II, the high luminosities and the slow rise/decay rates are thought to be explained by some of these four different power sources. A popular model is the interaction model, either by collisions between two dense shells—one with H and another without—ejected by PPISN (Woosley et al. 2007), or by strong interactions between ejecta and very dense H-rich CSM (Ofek et al. 2007; Smith & McCray 2007; Chevalier & Irwin 2011; Moriya & Maeda 2014). It is important to note that a combination of these power sources—magnetar, radioactive decay (PISN), CSM interaction, and PPISN—could work together to explain some SLSNe.

The explosion physics and power sources for SLSNe could be diverse, and the associated progenitor masses could also vary from $\sim 20 M_{\odot}$ (magnetar, Davies et al. 2009) up to $250 M_{\odot}$ (PISN). However, what is clear is that the progenitor stars of hydrogen-poor SLSNe must have lost most or all of their hydrogen envelopes prior to the supernova explosion. Possible causes of mass loss include massive wind and pulsational pair instabilities. A PPISN suggests the ejection of $10\text{--}20 M_{\odot}$ of H-rich material during each instability episode. This model naturally predicts that some SLSNe-I could have distant H-rich shells, previously lost due to the violent pulsational pair instabilities. At late times, the supernova ejecta

would eventually run into this distant H-rich shell, and produce broad Balmer emission lines from the interaction.

In this paper, we report for the first time the observations of two hydrogen-poor SLSNe with late-time spectral signatures of the ejecta interacting with an H-rich medium. We present a detailed analysis for iPTF13ehe that has extended photometric and spectroscopic data over 400 days. We summarize the results for the second source, PTF10aagc, at the end. The paper is organized as follows. The observational data is presented in Section 2, and the analysis and results are described in Section 3. In Section 4, we discuss the implications of these observations for various SLSN models.

Throughout the paper, we adopt a Λ CDM cosmological model with $\Omega_M = 0.286$, $\Omega_{\Lambda} = 0.714$, and $H_0 = 69.6 \text{ km s}^{-1} \text{ Mpc}^{-1}$ (Planck Collaboration et al. 2015).

2. OBSERVATIONS

iPTF13ehe was first detected as a transient source on 2013 November 25 by the intermediate Palomar Transient Factory (iPTF). Its equatorial coordinates are R.A. = 06:53:21.50, decl. = +67:07:56.0 (J2000). Using the observations presented below, we show that this event is at a redshift of 0.3434 and its photometric and spectroscopy properties are consistent with a hydrogen-poor, superluminous supernova, similar to SN2007bi. This section discusses the characteristics of the photometric and spectroscopic observations.

2.1. Photometric Data

The iPTF13ehe photometry was obtained mostly with the PTF survey Camera (Rahmer et al. 2008) on the 48 inch Oschin Schmidt telescope (P48) and the imaging camera on the robotic 60 inch (P60) telescope at Palomar Observatory (Cenko et al. 2006). Additional late-time photometry was obtained with the Large Format Camera (LFC) on the Palomar 200 inch (P200), the Keck, and the Discovery Channel Telescope (DCT). P48 data from 2013 February set useful constraints on the explosion date. The P48 images are processed by the PTF imaging processing pipeline written at the Infrared Processing and Analysis Center (IPAC; Laher et al. 2014). The photometry is measured using the PTF Image Differencing Extraction (PTFIDE) software (Masci 2014). This package produces both point-spread function (PSF) fitted photometry as well as aperture photometry on the reference-subtracted images. More importantly, co-added photometry and upper limits based on multi-epoch observations can be derived when the transient object is faint.

The photometry from the P60, the Keck Low Resolution Imager and Spectrograph (LRIS; Oke et al. 1995), and the DCT are measured through an appropriate aperture with diameter $(2\text{--}2.5) \times \text{FWHM}$ of the seeing disk. All photometry is in AB magnitudes, and calibrated onto the SDSS g , r , and i filters. On 2015 February 17, iPTF13ehe was observed by the *HST*/ACS/WFC camera in the F625W filter (PID: 13858) (A. de Cia et al. 2015, in preparation). The supernova iPTF13ehe is clearly offset from a faint dwarf galaxy. After the subtraction of the supernova light, the host galaxy photometry is 24.24 ± 0.06 mag (AB, r). The g -band decline is leveling out by 2015 March 23, with a total magnitude of 24.77. It faded only 0.1 mag during the two months between 2015 January 22 and March. Thus, we approximate the host brightness in g -band with 24.9. Some of the late-time photometry is taken with LRIS

Table 1
The g -, r -, and i -band Photometry

Julian Date (days)	r^a (mag)	σ (mag)	Julian Date (days)	g (mag)	σ (mag)	Julian Date (days)	i (mag)	σ (mag)
2456495.2	22.68	99.9 ^b	2456662.7	20.08	0.06	2456662.7	20.05	0.17
2456577.7	22.43	0.48	2456667.9	20.06	0.08	2456663.6	19.75	0.05
2456588.0	21.01	0.35	2456673.6	20.21	0.21	2456671.7	19.70	0.09
2456621.8	20.39	0.19	2456680.6	20.12	0.04	2456672.7	19.83	0.14
2456627.0	20.25	0.12	2456685.6	20.15	0.04	2456673.6	19.76	0.13
2456639.7	19.97	0.14	2456697.6	20.34	0.07	2456680.6	19.77	0.07
2456639.7	20.09	0.27	2456703.0	20.37	0.03	2456685.6	19.65	0.06
2456640.8	19.96	0.10	2456703.7	20.50	0.07	2456697.6	19.71	0.04
2456647.9	19.75	0.14	2456710.7	20.50	0.04	2456703.0	19.71	0.03
2456648.8	19.88	0.06	2456732.7	20.91	0.17	2456703.7	19.79	0.04
2456662.7	19.69	0.06	2456733.6	20.87	0.12	2456710.7	19.79	0.04
2456667.9	19.87	0.10	2456735.7	20.79	0.08	2456721.7	19.73	0.06
2456675.8	19.60	0.19	2456736.7	20.93	0.05	2456729.1	19.83	0.12
2456680.6	19.74	0.05	2456737.8	20.97	0.10	2456733.4	19.81	0.09
2456685.6	19.79	0.05	2456745.8	21.24	0.11	2456737.2	19.88	0.08
2456697.6	19.81	0.05	2456952.1	23.87	0.08	2456745.3	19.95	0.11
2456703.0	19.83	0.03	2456981.1	24.15	0.08
2456703.7	19.77	0.04	2457044.9	24.65	0.08
2456710.7	19.83	0.03	2457104.5	24.77	0.10
2456721.8	19.98	0.07
2456727.6	20.06	0.09
2456728.6	20.28	0.12
2456729.6	20.08	0.10
2456730.6	20.13	0.10
2456731.6	20.01	0.06
2456732.6	20.11	0.08
2456733.6	20.10	0.05
2456735.7	20.20	0.07
2456736.7	20.19	0.05
2456737.8	20.13	0.07
2456745.8	20.56	0.09
2456911.0	21.97	0.05
2456952.1	22.36	0.07
2456981.1	22.66	0.07
2457044.9	23.18	0.07
2457071.7	23.35	0.08
2457104.5	23.63	0.10

Notes.

^a The magnitudes include light from both the host and iPTF13ehe, and are in AB system. The host galaxy and the supernova are well separated in the *HST* images. The host galaxy r -band brightness is 24.24, measured from the *HST* photometry. The host g -band magnitude is set to 24.9 in the paper. The analysis in this paper does not use any late-time i -band photometry, thus the host subtraction is not critical. i -band host galaxy photometry has not been measured. All errors are in 1σ .

^b This r -magnitude is a 3σ limit.

Cousin R_c filter. We transformed R_c magnitude to SDSS r AB magnitude using the late-time spectra. The g , r , and i -band photometry are listed in Table 1. The tabulated photometry are not extinction corrected.

The Schlafly & Finkbeiner (2011) extinction map gives a Galactic extinction $E(B - V) = 0.04$ at the position of iPTF13ehe. We assume the extinction law of (Cardelli et al. 1989) with $A_V/E(B - V) = 3.1$. Specifically, A_g , A_r , and A_i are small, 0.14, 0.1, and 0.07 mag, respectively. In this paper, we have ignored any potential dust extinction from the host galaxy. This assumption is probably not too far off since most dwarf galaxies have low dust extinction and our late-time spectra do not show any significant reddening or NaD absorption lines. Studies of SLSN-I host galaxies also support this assumption (Lunnan et al. 2014; Leloudas et al. 2015).

2.2. Spectroscopy

Spectroscopic observations of iPTF13ehe were obtained on six epochs, three near the LC peak, and three during the late-time nebular phase (~ 300 days since the peak). The spectra were taken with the Keck Deep Imaging and Multi-Object Spectrograph (DEIMOS; Faber et al. 2003) and LRIS (Oke et al. 1995) mounted on the Keck 10 m telescopes, and with the Double Spectrograph (DBSP; Oke & Gunn 1983) on the P200. The spectral coverages are $\sim 3000\text{--}10000 \text{ \AA}$ and $4000\text{--}10000 \text{ \AA}$ for LRIS+DBSP and DEIMOS, respectively. The spectral resolution is moderate, with $\lambda/\delta\lambda \sim 800\text{--}2000$. DEIMOS observations were reduced using the software developed by the Deep Extragalactic Evolutionary Probe 2 (DEEP2) project (Newman et al. 2013). LRIS and DBSP observations were reduced by us (D. Perley and R. Quimby).

Table 2
The Spectroscopic Observation Log

Obs. Date	Julian Date (days)	Instrument	Exp. Time ^a (s)	Inst. Res. ^b (Å)
2014 Jan 01	2456658.5	Keck/DEIMOS	600	4
2014 Jan 06	2456663.8	P200/DBSP	1800	4.4
2014 Feb 01	2456689.9	P200/DBSP	1200	6.1
2014 Dec 17	2457008.4	Keck/LRIS	3100(blue), 2700(red)	5.6
2014 Dec 21	2457012.4	Keck/DEIMOS	6000	1.8
2015 Jan 22	2457044.4	Keck/LRIS	3800(blue), 1800(red)	5.6

Notes.

^a Keck/LRIS blue and red side exposure times are different.

^b Instrument spectral resolution is Full Width at Half Maximum (FWHM) and measured from unresolved sky lines.

using custom written software. The observation information is listed in Table 2.

All six spectra are flux calibrated and corrected for Galactic extinction assuming $E(B - V) = 0.04$ (see Section 2.1). We cross-check the spectral calibration against broadband photometry. Overall, the corrections to the spectral calibrations are small. The spectra taken near peak luminosity were not corrected for host galaxy contamination, since it is faint and negligible. For the late-time spectra, we perform host galaxy subtraction, as described below (Section 3.2). All calibrated spectra will be made publicly available via WISEREP (<http://wiserep.weizmann.ac.il>; Yaron & Gal-Yam 2012).

3. ANALYSIS AND RESULTS

3.1. LCs: Rise Time and Peak Bolometric Luminosity

Supernova LCs provide several important measurements that can constrain the explosion physics. This includes three observables: the rest-frame rise time from the date of explosion to the maximum brightness ($t_{\text{rise}}^{\text{rest}}$), the peak bolometric luminosity ($L_{\text{bol}}^{\text{peak}}$), and the post-peak decay rate ($\Delta M / \Delta t$).

Figure 1 illustrates the observed g , r , and i -band LCs as a function of Julian Date (JD). iPTF13ehe has a total of 48 images taken eight months prior to the discovery date on 2013 November 25. The upper limit and the two earliest detections in Figure 1 were derived from stacking, each using ~ 10 images spanning over 10 days. These early data—often missed for SLSNe—are very useful for constraining the rise timescale, the explosion date, and for searching for SN precursors (e.g., Ofek et al. 2014). The g - and r -band LCs are host-light subtracted, and the i -band LC covers only the peak epochs, which are not significantly affected by the faint host.

We first determined the peak and explosion dates using polynomial fits to the r -band LC. iPTF13ehe reached its peak at a Julian date (JD) of 2456670.77 days. Here we show how the explosion date, and thus rise time, can be affected by various factors. We define the explosion date as the time when the extrapolated r -band magnitude is fainter than 30 mag. When we use all of the data for a single polynomial fit (Figure 1; blue solid line), the derived explosion date is 2456471.3 days. But if we consider that the two earliest data points may favor a different rising slope, and fit the data with a piece-wise polynomial (red solid line), the derived explosion date is later, at JD = 2456522.5 days. The corresponding rest-frame rise times are $t_{\text{rise}}^{\text{rest}} = 148.5$ and 110 days, respectively. The large uncertainty is due to a lack of early observations, and more importantly, a lack of knowledge of the shape of early SLSN

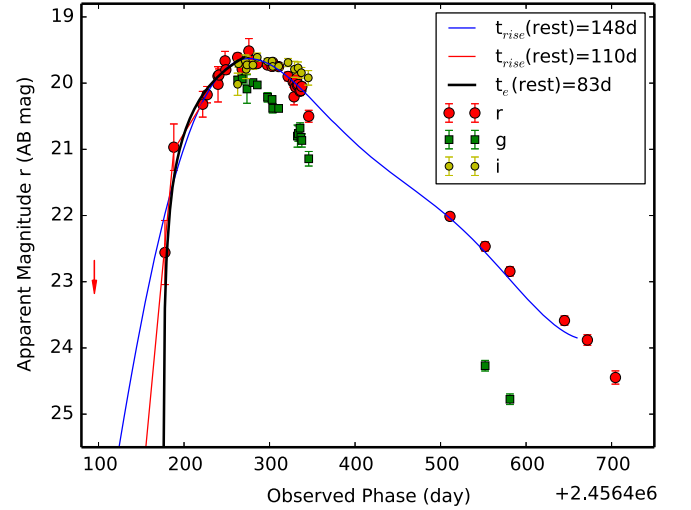


Figure 1. iPTF13ehe apparent brightness in the g -, r -, and i -bands vs. observed Julian date, overlaid with polynomial fits to the r -band LC in order to infer the peak and explosion dates. The blue line uses all of the data, the red line uses a piece-wise polynomial fit, and the black line is based on an exponential form. The timescales are in the rest-frame.

LCs. For example, instead of slower rising slopes indicated by the polynomial fit (blue and red lines in Figure 1), the early LC may have a faster rising exponential form of $L(t) = L_{\text{peak}}(1.0 - e^{-(t-t_0)/t_e})$, as applied to a sample of SN IIn in Ofek et al. (2014). The fit to the data yielded the explosion date $t_0 = 2456575.6$ days and the exponential rise time $t_e = 83$ days (shown as black line in Figure 1). The large uncertainty in $t_{\text{rise}}^{\text{rest}}$ illustrates one critical and the most difficult aspect of supernova observations—catch them early enough that the physical information can be derived. We conclude that the rise time $t_{\text{rise}}^{\text{rest}}$ is in a range of 83–148 days.

Rest-frame LCs require appropriate k -corrections. Here the k -correction, K_{QR} , is defined as $M_Q(\text{rest}) = m_R(\text{obs}) - \text{DM} - K_{QR}$, with the observed filter being R , the rest-frame filter being Q , and DM being the distance module. We transformed the observed r -band LC to rest-frame M_r and M_g LCs by applying K_{rr} and K_{gr} , calculated using the observed spectra at the three separated epochs (2014 January 06, 2014 February 01 and 2014 December 17). K_{gr} is -0.28 , constant for both the early and late epochs. The K_{gr} correction is almost constant because at $z = 0.3434$, the observed r filter samples rest-frame 4659.8 Å , very close to the g -band λ_{eff} at $z = 0$. Thus K_{gr} is

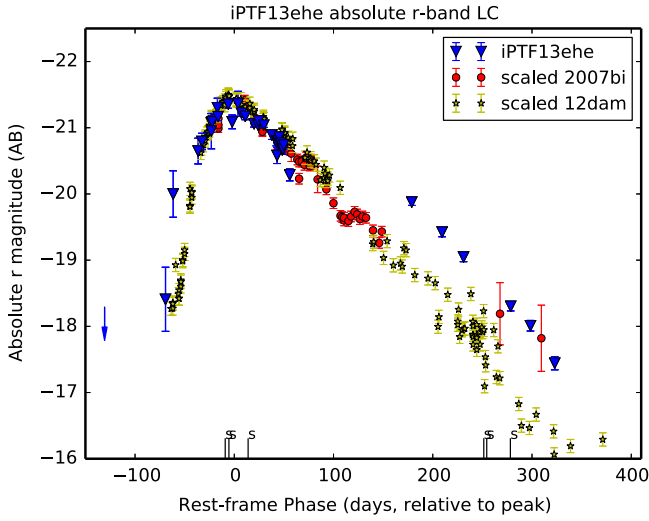


Figure 2. iPTF13ehe rest-frame, k-corrected M_r light curve in comparison with those of SN2007bi and PTF12dam (Gal-Yam et al. 2009; P. Vreeswijk et al. 2015, in preparation). The scaling factor is +0.1 mag for SN2007bi and 0.05 for PTF12dam.

approximately $2.5 \log_{10}(1+z)$ (for details see Hogg et al. 2002). The derived rest-frame M_g LC is shown in Figure 3.

K_{rr} is approximately -0.38 for the pre-peak photometry, -0.5 between the peak and $+100$ days post-peak (rest-frame), and $+0.54$ for the rest of the late-time photometry. We note that $K_{rr} = +0.54$ is the averaged value based on the three late-time spectra (see Figure 1). This K-correction is large and positive, making the rest-frame M_r LC brighter, as shown in Figure 2. The change of K_{rr} with time is due to (1) the emergence of a strong, broad $H\alpha$ emission line at late times (first detected at 2014 December 21); (2) the redder continuum in the supernova spectra. The large variation in K_{rr} is also responsible for the observed steep ($g-r$) color evolution with time, from 0.3 near the peak brightness to 1.5 at later times (Figure 1). How much of the M_r brightening is due to the continuum versus $H\alpha$? We test this by masking out the $H\alpha$ line from the late-time spectra and find that the calculated K_{rr} from the pure continua is $+0.3$, still quite significant.

The LCs shown in Figures 2 and 3 indicate a linear decline, except the brightening in the late-time M_r LC. The decay rates are 0.0155 and 0.0149 mag day $^{-1}$ for the r -band and g -band LCs, respectively. For the r -band LC, we measured the decay rate separately for the late-time and the post-peak photospheric period, and the values are very similar. These decline rates are much slower than those of any normal supernovae in the post-peak photospheric phases. We note that it is close to the pure ^{56}Co decay rate of 0.0097 mag day $^{-1}$.

Figures 2 and 3 compare the iPTF13ehe M_r and M_g LCs with those of SN2007bi and PTF12dam, two well-studied hydrogen-poor SLSNe (Gal-Yam et al. 2009; Nicholl et al. 2013; Chen et al. 2014). It is interesting to note that the decline rates of the three SLSNe are very similar, except for the elevated M_r bump in iPTF13ehe after the emergence of the broad $H\alpha$ emission. In addition, iPTF13ehe has a slower rising rate, and thus a wider LC compared to PTF12dam. One argument against PTF12dam being a pair instability supernova (PISN) is that its LC rose much faster than model predictions (Inserra et al. 2013; Nicholl et al. 2013).

The peak bolometric luminosity, $L_{\text{bol}}^{\text{peak}}$, is estimated as follows. We have g , r , and i photometry taken around the time

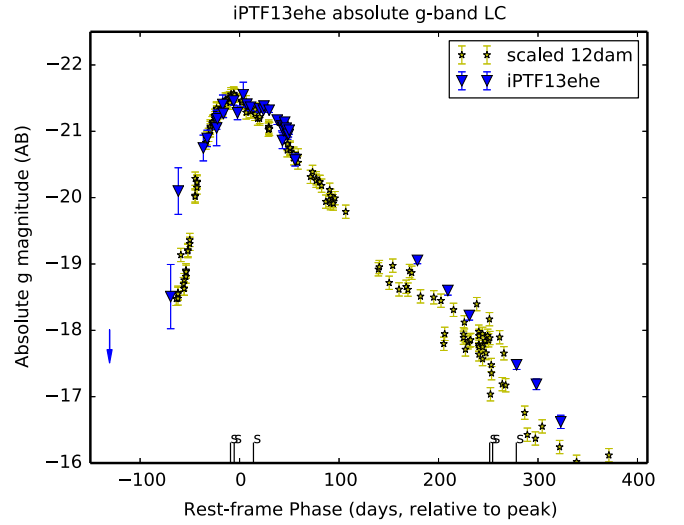


Figure 3. Comparison of the iPTF13ehe M_g LC with that of PTF12dam (P. Vreeswijk et al. 2015, in preparation). The PTF12dam g -band LC is shifted down by $+0.15$ mag.

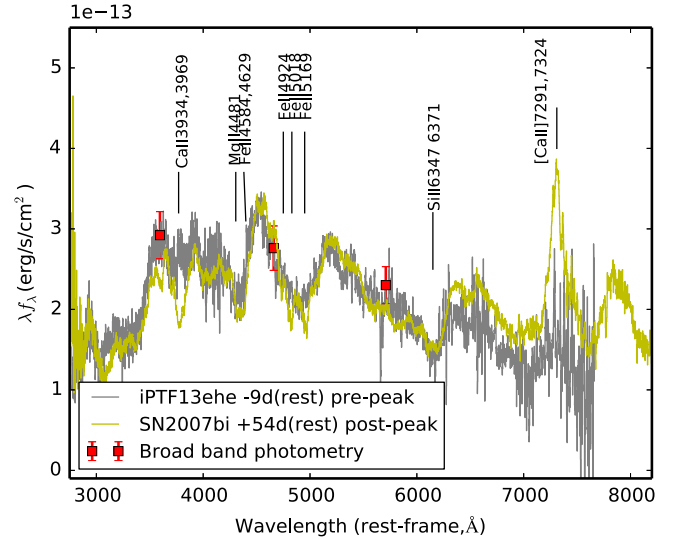


Figure 4. Optical spectrum during the photospheric phase of iPTF13ehe, taken at the pre-peak -9 days. We compare this spectrum with that of SN2007bi, which was proposed to be a PISN and powered by a large mass of ^{56}Ni (Gal-Yam et al. 2009).

when iPTF13ehe reached its peak brightness. Thus, we have fairly good estimates of the peak fluxes in these filters. The integral over the broadband defined SED between g - and i -band results in 6×10^{43} erg s $^{-1}$, which sets a lower limit on $L_{\text{bol}}^{\text{peak}}$. Figure 4 shows the spectrum in λf_{λ} versus λ_{rest} . This spectrum is taken at -9 days pre-peak. We used the broadband photometry taken nearest to this spectrum, and refined the flux calibration to account for slit losses. The continuum shape should reflect the blackbody radiation, and the bolometric flux f_{bol} is simply

$$f_{\text{bol}} = \int_0^{\infty} \left(\frac{2}{\lambda^2} \frac{h\nu}{e^{h\nu/k_B T} - 1} \right) d\nu = \frac{\sigma T^4}{\pi} = 1.386 \nu_m f(\nu_m), \quad (1)$$

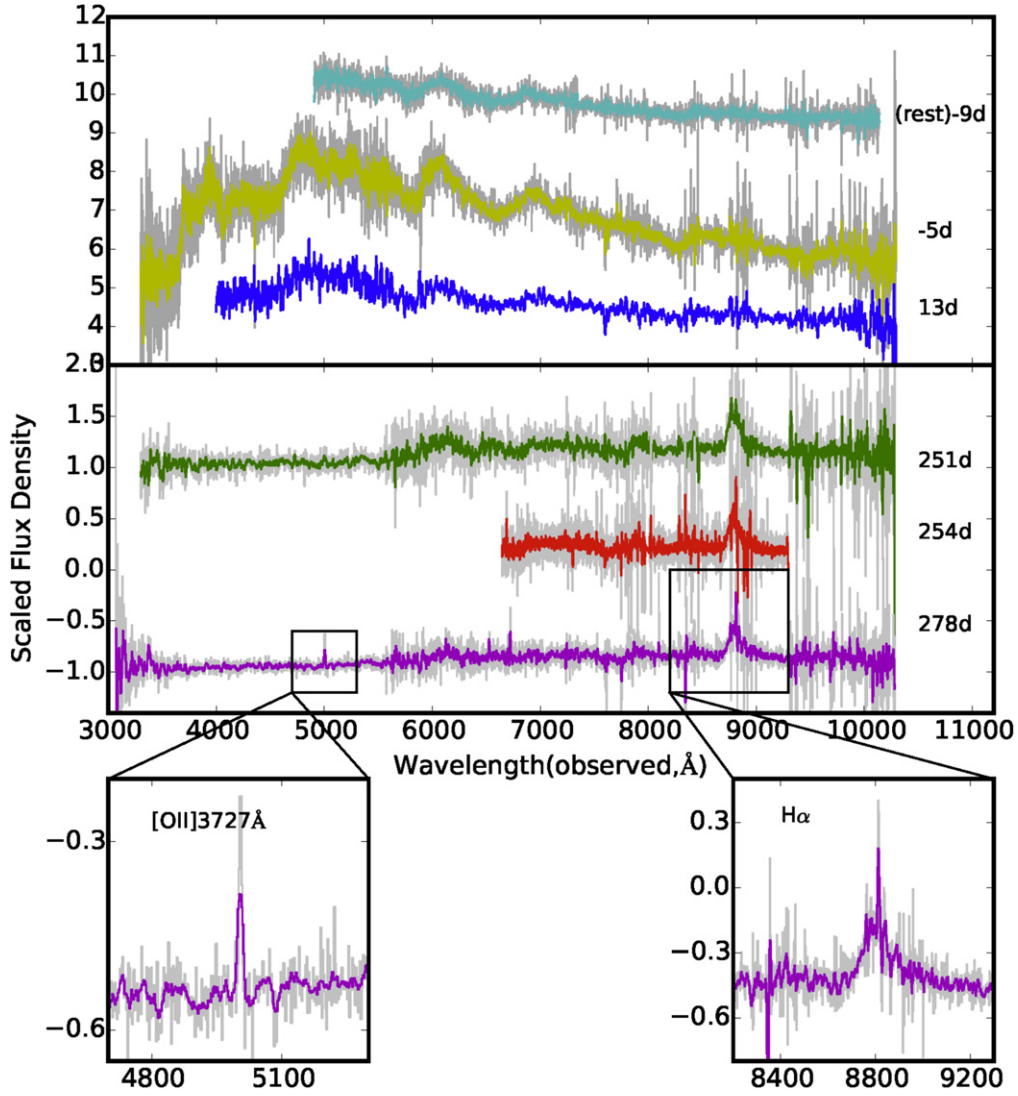


Figure 5. All six observed spectra are shown here with the rest-frame days relative to the peak brightness. For the third nebular spectrum taken at +278 days post-peak, we detected both broad and narrow H α components, as well as narrow [O II] 3727 Å. The color lines are the smoothed spectra. See the text for details on the smoothing lengths.

where ν_m is the frequency when νf_ν is at the maximum. From the spectra shown in Figure 4, λf_λ peaks at $\lambda \sim 4800$ Å, with $f_{\text{bol}} = 1.386 \lambda_m f_\lambda(\lambda_m) = 1.386 \times 4800.0 \times 4.95 \times 10^{-17} \text{ erg s}^{-1} \text{ cm}^{-2}$. This yields $L_{\text{bol}}^{\text{peak}} = 1.3 \times 10^{44} \text{ erg s}^{-1}$. This is consistent with the lower limit set by the broadband photometry.

With $t_{\text{rise}}^{\text{rest}}$ and $L_{\text{bol}}^{\text{peak}}$, it is clear that iPTF13ehe is an extremely luminous supernova. The total radiative energy can be estimated by, $E_{\text{rad}} \geq L_{\text{bol}}^{\text{peak}} \times t_{\text{rise}}^{\text{rest}} \sim 1.3 \times 10^{44} \text{ erg s}^{-1} \times 83 \text{ days} \sim 9.3 \times 10^{50} \text{ erg}$.

3.2. Photospheric and Nebular Phase Spectroscopy

iPTF13ehe was observed on six different epochs. Figure 5 presents these data, illustrating the evolution of the spectral features over the rest-frame time interval of 287 days. The color lines in the figure show the smoothed spectra, which are performed using astropy package `convolve.Box1DKernel` software. The smoothing length ranges from 6 to 8 Å (5–7 pixels) for the P200 and Keck LRIS spectra, and is much smaller, only 3 Å (11 pixels) for the DEIMOS high-resolution

spectrum (2014 December 21). In the section below, we discuss in detail the spectral properties in the photospheric and nebular phase separately. An accurate redshift is measured using the multiple narrow emission lines detected in the final spectrum (2015 January 22).

3.2.1. Photospheric Phase Spectra—Similarity between iPTF13ehe and SN2007bi

The earliest spectrum of iPTF13ehe, taken at $t_{\text{rest}}^{\text{peak}} = -9$ days pre-peak, is very similar to the earliest available photospheric spectrum (rest-frame +54 days post-peak) of SN2007bi, shown in Figure 4. No detectable H and He features are present, and the most prominent absorption features are from Mg II, Fe II, and Si II. This suggests that prior to the explosion, the progenitor star must have lost all of its hydrogen envelope, and the supernova explosion comes from the core containing heavier elements. Figure 4 illustrates that the width of the blended Fe II 5169 Å feature is very similar for these two spectra, allowing us to roughly infer the iPTF13ehe ejecta velocity of $\sim 12,000 \text{ km s}^{-1}$. This velocity is confirmed by

other methods. For example, it is thought that the blue minimum of the P-Cygni profile of Fe II 5169 Å is a fairly good indicator of the photospheric expansion velocity (Branch 2004). At an observed wavelength of 6620 Å, this feature implies $v_{ej} = 14,000 \pm 3000 \text{ km s}^{-1}$, with the error measured from the line profile fitting. Throughout the paper, we adopt $v_{ej} = 13,000 \text{ km s}^{-1}$, the averaged value between 12,000 and 14,000 km s^{-1} .

The significant spectral difference between SN2007bi and iPTF13ehe is around 7322 Å, where [O II] 7322 Å, [Ca II] 7291,7324 Å, [Fe II] 7155,7172,7388,7452 Å emission lines are located (Figure 4). iPTF13ehe probably has very weak Ca II 3934,3969 Å (H & K; absorption) and [Ca II] 7291,7324 Å (emission), in contrast to SN2007bi. Because the [Ca II] line is sensitive to gas density and is stronger at lower density, this may indicate that the ejecta of SN2007bi contains low density regions.

A simple blackbody fitting to the spectral continuum obtained at the epoch of -5 days produces a temperature T_{BB} of $\sim 7000 \text{ K}$. It is clear that near the peak, the optical spectra of iPTF13ehe are much flatter, i.e., cooler than those of PTF09cnd, an archetypical SLSN-I (Quimby et al. 2011). The earliest spectrum of PTF09cnd, taken at -20 days pre-peak, has a continuum blackbody temperature of $\sim 15,000 \text{ K}$ (Quimby et al. 2011). The cooler temperature in iPTF13ehe is also supported by the absence of O II 4072,4415,4590 Å absorption features (the O⁺ ionization potential is 35.1 eV, 40,000 K assuming thermal equilibrium). In contrast, O II absorptions are prominent in PTF09cnd (Quimby et al. 2011). Since SN2007bi does not have pre-peak spectra, it is possible that its earlier spectra may have a hotter continuum like PTF09cnd. However, this is not the case for iPTF13ehe since the first spectra were obtained prior to the peak epoch. Thus, it could be that sources like iPTF13ehe and SN2007bi may represent a different class of hydrogen-poor superluminous SNe, in the sense that they may have a different spectral evolution, suggesting different explosion physics. The detailed study of this issue will be presented in R. M. Quimby et al. (2015, in preparation), based on the full H-poor sample discovered by PTF from 2009 to 2012.

3.2.2. Nebular Phase Spectra—Detection of a Broad H α Emission Line

As Table 2 shows, we have three nebular-phase spectra taken on $t_{\text{rest}}^{\text{peak}} = +251, +254, \text{ and } +278$ days (post-peak) or $t_{\text{rest}}^{\text{exp}} = +322, +325, \text{ and } +349$ days (from explosion JD of 2456575.6 days) respectively. All three spectra display a strong, broad H α emission line with a velocity width $> 4000 \text{ km s}^{-1}$, as well as a narrow H α emission component. Below we discuss in turn the nature of these two components.

The first question is whether the narrow H α component is from the recombination of ionized hydrogen atoms in a slow-moving shell or from the host galaxy. This type of narrow emission feature is commonly seen in the spectra of SN II_n and usually comes from the slow-moving, outer layer of the H-rich CSM surrounding the supernova. In the case of iPTF13ehe, the complication comes from the fact that all available spectra contain signals from both the supernova and the host galaxy. In the three nebular spectra, the narrow H α line is unresolved for the two spectra taken with LRIS and resolved in the high-resolution DEIMOS data (FWHM of 1.8 Å) taken on 2014 December 21. The integrated line fluxes for the narrow

component are 2.2×10^{-17} , 2.1×10^{-17} , and $3.88 \times 10^{-17} \text{ erg s}^{-1} \text{ cm}^{-2}$ for 2014 December 17, 21 and 2015 January 22, respectively. The January 2015 spectrum has the highest signal-to-noise ratio (S/N) and also detects H β and narrow [O II] 3727 Å emission lines. The redshifts inferred independently from the narrow H α and [O II] lines are the same, at $z = 1.3429$. The integrated [O II] 3727 Å line flux is $2.64 \times 10^{-17} \text{ erg s}^{-1} \text{ cm}^{-2}$, implying an SFR of $0.15 M_{\odot} \text{ yr}^{-1}$ based on the conversion from Kennicutt (1998). If all of the narrow H α line flux ($3.88 \times 10^{-17} \text{ erg cm}^{-2}$) comes from star formation, the inferred SFR is $0.13 M_{\odot} \text{ yr}^{-1}$, 15% lower than that inferred from [O II].

The observed flux variations with time in the narrow H α line are likely due to the combination of the weather changes and different slit position angles. The consistent redshift and SFR measured from [O II] and narrow H α suggest that the narrow H α line is mostly from the host galaxy and not from the supernova. Additional support for this conclusion comes from the high-resolution DEIMOS spectrum taken on 2014 December 21. Figure 6 shows the reduced, two-dimensional spectrum around the H α region. We found that the narrow H α component is resolved in velocity, and is consistent with the host galaxy rotation velocity field of 65 km s^{-1} (roughly 1 spectral resolution, 1.8 Å). Furthermore, the top panel of Figure 6 shows the DEIMOS slit overlaid on the direct image of iPTF13ehe (red dot) and the host galaxy. The narrow H α with extended velocity (the bottom panel) does not have any obvious strong emission corresponding to the spatial location of iPTF13ehe (south of the center of the host galaxy). We therefore conclude that the narrow H α line is most likely from the host galaxy of iPTF13ehe.

The final piece of evidence supporting this conclusion is discussed in Section 4.2 below, where we argue that the H-rich CSM shell is likely to be mostly neutral because of the shell mass limit constraint by the Thomson optical depth ≤ 1 in the nebular phases.

For the remainder of this section, we present our analysis of the broad H α component. Figure 7 presents the first nebular spectrum ($t_{\text{rest}}^{\text{exp}} = +322$ days) in comparison with the spectrum of SN2007bi taken at a similar phase. The strongest feature in the iPTF13ehe spectrum is its broad H α , whereas that of SN2007bi has no traces of either H α or H β from the supernova. This broad H α line is likely produced when the iPTF13ehe ejecta run into a H-rich CSM and the kinetic energy is converted into thermal emission, a part of which escapes in the H α and H β lines. It is intriguing that the emission from the [O I] 6300,6363 Å is very weak or absent, whereas this feature is very strong in SN2007bi. The cooling ejecta from iPTF13ehe also produced emission such as broad [Mg I] 4570 Å, a possible blend of Na 5890 Å + He I 5876 Å lines, and a blend of broad Fe II 5169, 5261, 5273, 5333 Å. The weak broad feature around 4861 Å could be H β , with a similar physical origin as that of H α .

We note that the host galaxy starlight was subtracted from the observed spectra as follows. The host spectrum is constructed using a Bruzual–Charlot model (Bruzual & Charlot 2003), constrained to have the same star formation rate (SFR) measured from the narrow [O II] 3727 Å from the host galaxy. The continuum decrement around 4000 Å is also used to match the model host spectrum. Our data is inadequate for determining if a fraction of the narrow H α emission line is from the supernova.

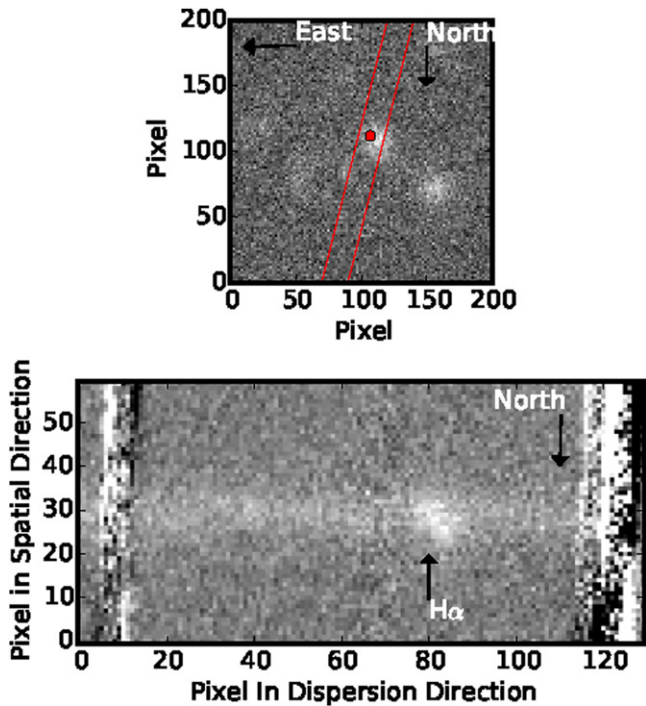


Figure 6. Top panel: the DEIMOS slit (red lines) with a position angle (PA) of 200 overlaid on iPTF13ehe (red dot) and the host galaxy. The slit width is $1''/2$. Bottom panel: the reduced two-dimensional DEIMOS spectrum taken on 2014 December 21. The x -axis is the dispersion direction, with a scale of $0.33 \text{ \AA pixel}^{-1}$, and the y -axis is the spatial direction, with a scale of $0''.1185 \text{ pixel}^{-1}$.

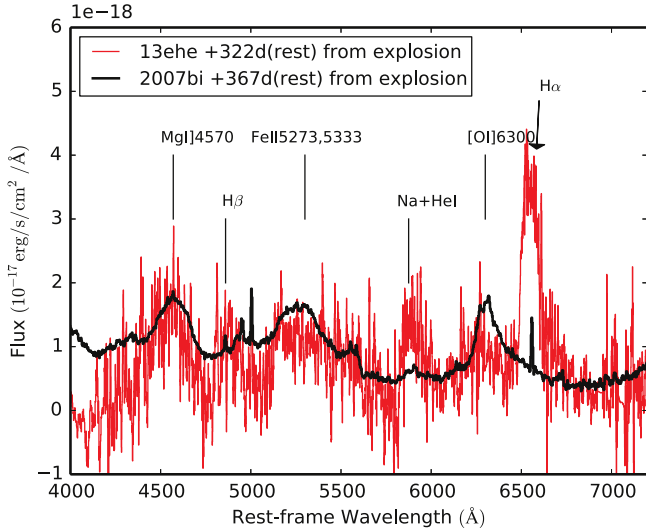


Figure 7. Optical nebular-phase spectrum of iPTF13ehe, taken +322 days (rest-frame) from the estimated explosion date. We compare this spectrum with that of SN2007bi, which was taken at +367 days (rest-frame) from the estimated explosion date, downloaded from WISEREP (Gal-Yam et al. 2009; Yaron & Gal-Yam 2012).

We fit Gaussian profiles to both the broad and narrow $H\alpha$ lines in the spectra, shown in Figure 8. The broad component has an FWHM between 3870 and 4850 km s^{-1} , which did not change much between 2014 December 17 and 2015 January 22. The integrated $H\alpha$ fluxes are $5.2\text{--}3.8 \times 10^{-16} \text{ erg s}^{-1} \text{ cm}^{-2}$, implying $L_{H\alpha} = 2.2\text{--}1.6 \times 10^{41} \text{ erg s}^{-1}$, decreasing by 20% over a period of 60 days. We also measured the velocity shifts

between the narrow and broad components, $\delta v \sim 410$ and 230 km s^{-1} for the LRIS spectra taken on 2014 December 17 and 2015 January 22.

Finally, we conclude that the broad component is from the SN ejecta interaction with an H-rich CSM, similar to the intermediate-velocity-width Balmer lines frequently observed among SN IIn. The $\sim 4000 \text{ km s}^{-1}$ of the broad component indicates the thermal, random motion of the shock-ionized H atoms. We assume that the velocity difference between the broad and narrow component, $\sim 300 \text{ km s}^{-1}$, is the H-shell systematic velocity. This assumption affects the calculations of the shell radius and when the shell is ejected by the progenitor star. We speculate that the velocity shell cannot be much larger than a few 100 km s^{-1} , otherwise the wavelength center of the broad component would be significantly shifted from the host galaxy redshift. However, it is possible that the shell could move slower than what we assumed.

3.2.3. Nebular Emission Models

A nebular emission model was computed for two epochs of the iPTF13ehe spectra (2014 December 17 and 2015 January 22) using the code described in Mazzali et al. (2007). The code computes the heating of SN ejecta following the deposition of γ -rays and positrons from ^{56}Ni and ^{56}Co decay, balancing this by cooling via line emission in non-local thermodynamic equilibrium (NLTE).

In the case of iPTF13ehe, given the low S/N of the nebular spectra, line profiles could not be modeled, so a one-dimensional (1D) version of the code was used. The model spectra are compared with the observed data in Figure 9. Line width was matched to an ejecta velocity inside which all emission was assumed to occur. This velocity is quite low, 4000 km s^{-1} . The intensity of the Fe emission in the blue was used to determine the mass of ^{56}Ni , which also depends on cooling from other species. The $[\text{O I}] 6300, 6363 \text{ \AA}$ emission line is unusually weak in iPTF13ehe in comparison with the nebular spectra of SN2007bi and other SN Ic events. Ignoring all material at velocities above 4000 km s^{-1} , we obtain a reasonable match to the spectra (excluding $H\alpha$) for $M(^{56}\text{Ni}) \sim 2.5 M_{\odot}$. This would correspond to a progenitor star of $\sim 95 M_{\odot}$ in the models of Heger & Woosley (2002). However, the oxygen mass in our model is only $13 M_{\odot}$, much less than the predicted value of $45 M_{\odot}$ (Heger & Woosley 2002). Although more oxygen may be located at velocities above 4000 km s^{-1} and may not be significantly excited by radiation coming from the core. It is possible that a significant part of the CO core of the star was lost before the explosion. This is clearly in contradiction to the Heger & Woosley (2002) model prediction. In addition, we have kept the masses of Si and S at the values of the $95 M_{\odot}$ model of Heger & Woosley (2002; 20 and $8 M_{\odot}$, respectively). This leads to strong cooling lines of these elements, which are not in contradiction with the optical data but are predicted to be very strong in the near-infrared, which is unobserved. Should these elements be reduced in mass, the ^{56}Ni mass would also be reduced. This naive comparison of model and data is to illustrate the obvious limitations and contradictions in the existing models of SLSNe. In the case of iPTF13ehe, the lack of any $[\text{O I}] 6300 \text{ \AA}$ emission imposes a challenge to the models assuming massive progenitors.

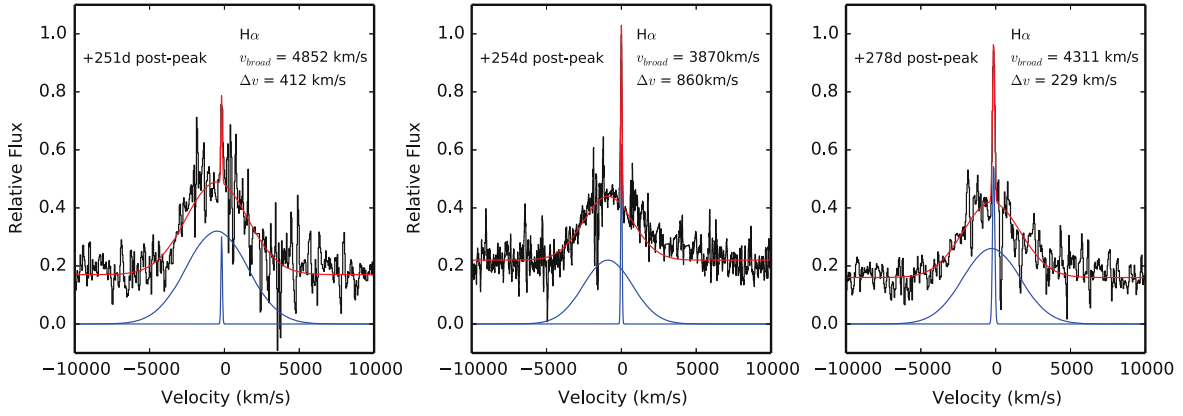


Figure 8. Gaussian profile fitting to the broad and narrow H α lines for the three epochs at +251, +254, and +278 days post-peak.

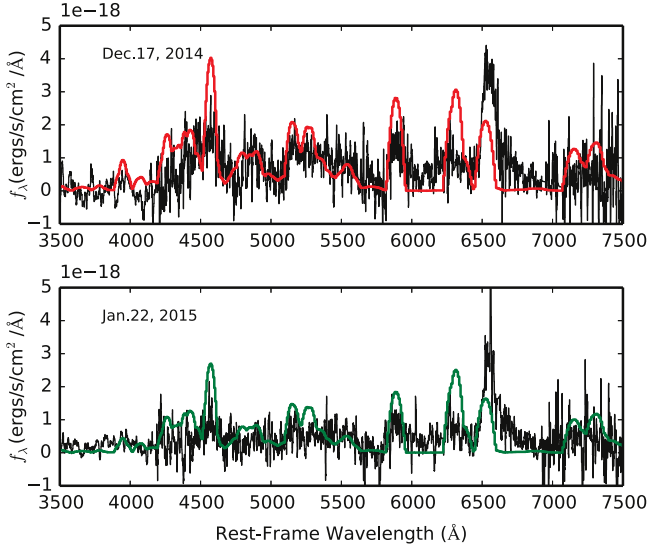


Figure 9. 1D nebular emission line models plotted against the spectra taken on two different epochs separated by a month. The colored spectra are model predictions and the black lines are observed spectra.

4. DISCUSSIONS

4.1. Physical Characteristics of the Explosion

The LCs and spectra provide measurements of $t_{\text{rise}}^{\text{peak}}$, $L_{\text{bol}}^{\text{peak}}$, and v_{ej} , which allow us to make the following physical parameter estimates.

We begin with the supernova ejecta mass M_{ej} . The SN rise time is determined by how long it takes photons to radiatively diffuse out to the emitting surface. This radiative diffusion time t_{diff} can be derived based on electron Thomson scattering and expressed in terms of M_{ej} , $t_{\text{diff}} = f(\kappa M_{\text{ej}}/Rc)$, where $f = \frac{9}{4\pi^3}$ and κ is mass opacity in $\text{cm}^2 \text{g}^{-1}$ (Arnett 1996; Padmanabhan 2000). The characteristic timescale for a supernova LC is defined as $t_c = \sqrt{2t_h t_{\text{diff}}}$, where t_h is hydrodynamic scale, R/v_{ej} . Thus, $t_c = \sqrt{2f\kappa M_{\text{ej}}/(c \times v_{\text{ej}})}$.

This equation is the basis for an empirical scaling relation, $t_{\text{rise}}^{\text{rest}} \propto t_c \propto \sqrt{(M_{\text{ej}}/v_{\text{ej}})}$. Using this relationship and another well-studied Type Ib event, SN 2008D, with $v_{\text{ej}} = 10,000 \text{ km s}^{-1}$, $t_{\text{rise}}^{\text{rest}} = 19$ days, and $M_{\text{ej}} = 7 M_{\odot}$ (Mazzali et al. 2008), we derive $M_{\text{ej}}(\text{iPTF13ehe}) = 173 M_{\odot}$. Using $t_c \simeq t_{\text{rise}}^{\text{rest}}$, we calculate $M_{\text{ej}} \sim 67\text{--}219 M_{\odot}$ assuming $\kappa = 0.1 \text{ cm}^2 \text{g}^{-1}$ for an ejecta composed of heavy elements.

The mass opacity (κ) due to electron scattering is determined by the ionization fractions of C, O, and Fe, as well as line opacity. For ejecta composed of heavy elements, various studies have used κ in the range of $(0.01\text{--}0.2) \text{ cm}^2 \text{g}^{-1}$ (Arnett 1982; Bersten et al. 2011, 2012). The M_{ej} estimate is quite sensitive to κ and t_c , which are very uncertain with our current knowledge. Regardless of the large uncertainty in M_{ej} , we can conclude that the exploding core mass of iPTF13ehe is $>67 M_{\odot}$. This implies that the progenitor star of iPTF13ehe must be very massive.

The second physical parameter is the supernova kinetic energy, $E_{\text{kin}} = \frac{1}{2}M_{\text{ej}}v_{\text{ej}}^2 = 0.5 \times (67\text{--}220) M_{\odot} \times (13,000)^2 \text{ km s}^{-1} = (1\text{--}4) \times 10^{53} \text{ erg}$. The implied kinetic energy E_{kin} to the ejecta mass M_{ej} ratio in units of $10^{51} \text{ erg per } 1 M_{\odot}$ is ~ 1.6 . Comparing to the lower limit on the supernova radiative energy, $E_{\text{rad}} \geq 0.93 \times 10^{51} \text{ erg}$, this implies that $<1\%$ of E_{kin} is being converted into visible radiation. Most of the kinetic energy from this extreme power explosion has gone into expansion.

Our inferred E_{kin} is extreme in comparison with typical values observed among Type Ia and core-collapse SNe. Specifically, for a normal core-collapse supernova, the total gravitational energy available from forming a neutron star is of an order of 10^{53} erg , and a very large fraction of that is lost to free-streaming neutrinos. So it is difficult to explain within a standard core-collapse model how iPTF13ehe could get such an extremely large kinetic energy. This imposes a challenge to models that use magnetars as energy sources. One possible mechanism for producing such a large explosion energy is PPISN or PISN models for the most massive stars from Heger & Woosley (2002). However, we note that it is also possible that the ejecta mass M_{ej} is overestimated by a factor of (5–10). As discussed earlier, the commonly used methods have serious limitations, and it is not clear how to measure ejecta masses more accurately for SLSN events.

The third physical parameter is the ^{56}Ni mass. If the power source for the observed luminous emission is radioactive decay of ^{56}Ni , how much of this material would be required? The bolometric peak luminosity, $1.3 \times 10^{44} \text{ erg s}^{-1}$, can constrain the amount of ^{56}Ni and ^{56}Co , based on $L_{\text{bol}} = 8 \times 10^{42} \text{ erg s}^{-1} \times M_{\text{Ni}}/M_{\odot}$ (Arnett 1982; Smith et al. 2007). The inferred M_{Ni} is $16 M_{\odot}$. Katz et al. (2013) discussed another method, $\int_0^t Q(t')t'dt' = \int_0^t L_{\text{bol}}(t')t'dt'$, with $t \gg 40$ days, Q as the radioactive heating function ($^{56}\text{Ni} \rightarrow ^{56}\text{Co} \rightarrow \text{Fe}$), and can be expressed as

$Q(t) = 3.9 \times 10^{10} e^{-t/7.6e+5} + 6.78 \times 10^9 (e^{-t/9.59e+6} - e^{-t/7.6e+5})$. All are in cgs units. Using this relation and the r -band absolute magnitude LC, we derive a lower limit on M_{Ni} of $13 M_{\odot}$. These numbers are much larger than those of any classical supernovae. The calculations assuming ^{56}Ni as the single power source yield much larger estimates than the prediction from our nebular emission model. This may indicate that multiple power sources could be in play for producing the iPTF13ehe emission. Radioactive decay could be one of them, and the total ^{56}Ni mass does not have to be so extremely large.

Finally, if the emission at the peak luminosity is considered to be a blackbody, the energy can be estimated as $E_{\text{rad}} = \frac{4\pi}{3} R_{\text{ph}}^3 \times a T_{\text{eff}}^4$, where R_{ph} is the photospheric radius at the peak luminosity, and T_{eff} is the blackbody effective temperature. As discussed in Section 3.2.1, T_{eff} is quite low, 7000 K. With the lower limit on E_{rad} , this equation implies that the size of the photosphere is $R_{\text{ph}} \sim 1.8 \times 10^{16}$ cm, a very large radius at peak luminosity compared to that of normal SNe. This is mostly due to the low value of T_{eff} . It is not clear why some SLSNe-I seem to have much cooler temperatures at similar early phases than others.

4.2. What Produced the Broad H α Emission in the Late-time Spectra?

The key new result we present here is the discovery of a broad H α line with a velocity width of 4000 km s^{-1} in the late-time spectra. The question is how this emission might be produced. The simple explanation is the interaction of the SN ejecta with a H-rich CSM, as commonly seen in SLSN-II spectra. However, the key difference here is that this H-rich material is in a shell, located at a distance much further away from the explosion site. The reason for a discrete shell rather than continuous CSM material such as wind-driven mass loss is because the early-time spectra do not show any signatures of the ejecta-CSM interaction. This interaction only appears at late times.

At the rest-frame -9 days pre-peak, the SLSN ejecta velocity was $13,000 \text{ km s}^{-1}$. Let us take the estimated explosion date as 2456575.6 days (the latest explosion date from the exponential fit). The first detection of H α is on JD = 2457008.5, giving an interval in the rest-frame $\Delta t_{\text{rest}} = 322$ days. As Figure 2 shows, there is no spectroscopy between $+13$ and $+251$ days (post-peak, rest-frame), therefore the precise time when H α emission lines first appear cannot be determined. The date of the third spectrum without H α (JD = 2456689.5) can be used to set the lower limit on $\Delta t_{\text{rest}} = 85$ –322 days. In practice, the lower limit value of 85 days is unlikely. In the rest of the calculations we use only $\Delta t_{\text{rest}} = 322$ days for simplicity. Assuming that the ejecta did not slow down significantly before running into the CSM shell, the approximate distance traveled by the ejecta is $R_{\text{rest}} = v_{\text{ej}} \times \Delta t_{\text{rest}} = 4e + 16$ cm. The broad H α line has a width of $\sim 4000 \text{ km s}^{-1}$, and is separated from the narrow H α by roughly $(400\text{--}230) \text{ km s}^{-1}$. We interpret the 4000 km s^{-1} line width as the thermal motion of shock-ionized hydrogen atoms, and the velocity shift of $\sim 300 \text{ km s}^{-1}$ is v_{CSM} , the CSM shell velocity. We can set a limit on the timescale, Δt , when this material was ejected by the progenitor star, using $\Delta t \times v_{\text{CSM}} = R_{\text{rest}}$, giving $\Delta t^{\text{rest}} \leq 40$ years. This is an upper limit since the CSM shell could initially have had a higher speed.

Let us consider an H-rich CSM shell with a radius of 4×10^{16} cm surrounding iPTF13ehe. This naturally begs two questions: (1) is this material from the progenitor star or a part of the galactic ISM? and (2) why does this CSM not produce any observable signatures—either in emission or absorption—in the early spectra when the UV photons from the early explosion would have interacted with this material?

This H-rich CSM shell is only 4×10^{16} cm from the location of the progenitor star, which is several orders of magnitudes smaller than the typical size of a H II region. Therefore, this H-rich CSM is probably not a part of the galactic ISM, but rather more likely produced by either wind mass loss or ejection due to some other mechanism, such as pulsational pair instability, occurring in massive stars ($>67 M_{\odot}$).

As early as—days pre-peak, the follow-up spectra reveal strong supernova signatures, which implies that at this phase, the CSM shell must be optically thin to visible photons. The fact that we also do not detect any narrow hydrogen recombination lines from the H-rich CSM shell, commonly seen in the spectra of SN IIn, could suggest two possibilities. First is that this H-shell had already become neutral when the first spectrum was taken. Second is that this H-shell is ionized, but the early spectra are dominated by the supernova light, and the exposure times are too short to detect any H-recombination signals from this ionized shell. However, as shown below, this second scenario is unlikely because of a short recombination timescale.

When this CSM shell was initially ejected by the progenitor star 50 years ago, the medium was very likely fully ionized. This ionized state was maintained by the heat sources from the progenitor star, and probably continued to the early phase of the supernova explosion. However, when the supernova photosphere cools down, there are no more heat sources and the ionized H atoms in this shell will recombine. This recombination timescale must be less than 62 days (rest-frame, from the explosion date of 2456575.6), i.e., the recombination is completed before the date of the first optical spectrum. Assuming Case B recombination, the recombination timescale is $t_{\text{rec}} \sim 10^{13}/n \text{ s} < 62$ days, with n being the volume density, and $n = M_{\text{CSM}}/4\pi m_{\text{H}} R_{\text{rest}}^2 w$, $R_{\text{rest}} = 4 \times 10^{16}$ cm (radius of the shell), m_{H} as the hydrogen mass, and w as the width of this shell. Assuming that the shell width w is only 10% of the shell radius, the above equations yield $M_{\text{CSM}} > 0.03 M_{\odot}$.

As shown below, the shell mass M_{CSM} is constrained to be $< 30 M_{\odot}$. At the upper limit of $30 M_{\odot}$, the H-recombination timescale $t_{\text{rec}} \sim 10^5 \text{ s}$. Thus, at the early phases of the spectral observations, the H-shell is already neutral.

Once this CSM shell becomes neutral, without any other heat sources, it stays neutral until the SN ejecta run into this shell. The shock front generates high-energy photons that ionize the hydrogen atoms again. These ionized H atoms recombine, and produce the observed H α and H β emission lines. The important question is if this shock-ionized shell (or partially ionized shell) is optically thick to Thomson scattering. The fact that the late-time spectra do display SN spectral signatures, such as [Mg I] 4570 Å, suggests that this shock-ionized shell is probably not optically thick to Thomson scattering. Other evidence that the CSM shell is not extremely dense comes from the *SWIFT* soft X-ray observation taken on 2014 December 23, yielding a 3σ limiting luminosity of $3 \times 10^{43} \text{ erg s}^{-1}$. In addition, the ejecta interaction with extremely dense CSM

would produce elevated continuum emission, which is not observed in the late-time absolute g -band LC.

So if the shock-ionized CSM shell is optically thin, we have $\tau_{\text{thomp}} = \kappa \rho w \leq 1$, where ρ is the density, and w is the width of this CSM shell. With $\rho = \frac{M_{\text{csm}}}{4\pi R^2 w}$, the above equation is simplified as $M_{\text{csm}} \leq \frac{4\pi R^2}{\kappa}$, independent of the width of this shell. Assuming $\kappa = 0.34 \text{ cm}^2/\text{g}$ for an H-rich medium, we have $M_{\text{csm}} \leq 30 M_{\odot}$. This mass value corresponds to a volume number density and a column density of $4 \times 10^8 \text{ cm}^{-3}$ and 10^{24} cm^{-2} , respectively. We predict that this shell should produce strong Ly α absorption features if any UV spectra were taken. There should not be much H α absorption because without an external excitation source, most of the H atoms are in the $n = 1$ ground state. To have a significant population in the $n = 2$ state with collisional excitation, it would require the gas to have a very high temperature, such that $KT \sim \Delta E_{21} = 10 \text{ eV} \sim 100,000 \text{ K}$. The shell around iPTF13ehe is unlikely to have such a high temperature.

With the estimated M_{csm} , we can calculate the kinetic energy of this CSM shell, $\frac{1}{2} M_{\text{csm}} v_{\text{csm}}^2 = 2 \times 10^{49} \text{ erg s}^{-1}$. Here we assume that the CSM shell systematic velocity is $\sim 300 \text{ km s}^{-1}$, roughly the velocity shift observed between the broad and narrow H α lines. The initial v_{csm} could be larger. The energetics of this shell is within the predictions of PPISN models (Woosley et al. 2007).

We note that the CSM shell may be partially ionized. This would lead to higher M_{csm} value and suggests that collisional excitation might be important for producing H α . The shock heated CSM shell with Balmer dominated emission is a complex system. The broad H α emission is likely produced by charge exchange between fast moving neutral H atoms (Chevalier et al. 1980; Morlino et al. 2013). Better quantitative estimates will need to apply the theory of Balmer dominated emission shock. This is beyond the scope of this paper.

4.3. iPTF13ehe: Pulsational Pair Instability Supernova (PPISN) versus Other Models

Detection of a H-rich CSM shell around a H-poor SLSN is a natural prediction from the PPISN model (e.g., Woosley et al. 2007; Waldman 2008). Table 1 in the supplemental material from Woosley et al. (2007) illustrates that in the cases of He-core masses greater than $53 M_{\odot}$, the time interval between the first and the second instability pulses could be as long as $6 \times 10^9 \text{ s}$, and the subsequent instabilities would happen more frequently. iPTF13ehe lost its H-shell about 40 years (10^9 s , rest) before the SN explosion. In addition, the kinetic energy of this CSM shell is about $2 \times 10^{49} \text{ erg s}^{-1}$, similar to what is predicted in Table 1 of Woosley et al. (2007). Both the timescale and energetics support the hypothesis that iPTF13ehe could be a PPISN candidate. In this scenario, iPTF13ehe started with a progenitor star with an initial mass of $>70 M_{\odot}$, ejected about $<30 M_{\odot}$ from the H envelope about 40 years ago (rest), during the first episode of pulsational pair instability. Following the first mass ejection, there is at least one, possibly more pulsational pair instabilities before the supernova explosion. The later ejected H-poor CSM shell tends to be faster and more energetic than the previous one, naturally leading to shell-shell collision (Woosley et al. 2007). The reason for possible additional instability pulses is that the H-poor CSM shell-shell collision could provide one of the power sources for the observed LC and spectral features.

However, this PPISN model could have one potential problem. The highest kinetic energy generated by these pulsational pair instabilities is predicted to be $8 \times 10^{50} \text{ erg}$, no more than 10^{51} erg . The relative kinetic energy between the 2nd and 3rd pulses would be even smaller. Therefore, even with the most efficient kinetic and thermal energy conversion, it may be hard to produce the peak radiative energy measured for iPTF13ehe ($>9.3 \times 10^{50} \text{ erg}$). One solution proposed in Quimby et al. (2011) is that after several episodes of pulsational pair instabilities, the core undergoes supernova explosion. The ejecta interaction with the last H-poor CSM shell could provide a more energetic reservoir for powering the observed emission. This is derived from an earlier idea proposed for SLSNe-II by Woosley et al. (2007).

The second caveat regarding the PPISN model is that the spectra of iPTF13ehe do not show much [O I] 6300 Å emission in all of the phases for which we had data. The iPTF13ehe ejecta seems not to have much oxygen material. This is clearly in contradiction with the models calculated by Heger & Woosley (2002), which predict an oxygen-dominated core with the mass $>50 M_{\odot}$. Our estimated ejecta mass has a lower limit of $70 M_{\odot}$, suggesting a very massive core. However, this calculation depends on the assumed value of opacity, κ . If adopting a higher value of 0.2, the ejecta mass would be a factor of two smaller. These uncertainties may suggest a less massive progenitor star that does not go through pulsational pair instabilities. For example, a luminous blue variable (LBV) could eject a massive H envelope from the progenitor star during its instability episode, like Eta Carina. Then a massive core-collapse model, such as the one proposed by Moriya et al. (2010), is needed to explain the energy output of iPTF13ehe.

With very low metallicity and rotation, a variation of the PPISN model could have a progenitor star with a much lower mass than the 95–150 M_{\odot} predicted in the Woosley et al. (2007) study. As pointed out in the studies of Chatzopoulos & Wheeler (2012) and Yoon et al. (2012), low metallicity and rotating stars could undergo pulsational pair instabilities at initial stellar masses as low as ~ 50 – $70 M_{\odot}$. Our constraint on the iPTF13ehe progenitor mass is not very stringent; the lower limit is less than the initial mass of $95 M_{\odot}$ predicted by the Woosley et al. (2007) model. If low metallicity and rotation are relevant, iPTF13ehe could be a PPISN candidate.

Finally, there is another alternative physical model, which was briefly mentioned in Woosley et al. (2007). A 95–150 M_{\odot} star with rotation and magnetic torques would initially evolve in a similar fashion to one without rotation and magnetic field. It will undergo episodes of pulsational pair instability that eventually produce a C/O core with a mass in the range of 40–60 M_{\odot} . However, the difference is that the rotating star with magnetic torque can end up forming a neutron star with a fast spin-period of a few milliseconds and a magnetic field strength of 10^{15} G —i.e., a magnetar (Duncan & Thompson 1992; Heger et al. 2005). The spin-down of a magnetar can provide sufficient power for a SLSN, as shown in several studies (Kasen & Bildsten 2010; Inserra et al. 2013; Nicholl et al. 2013). For iPTF13ehe, it is possible that its massive progenitor star experiences several episodes of pulsational pair instabilities, ejecting several shells, and the final supernova explosion leaves behind a magnetar. The power sources for the observed LC and early-time H-poor spectra could well be a combination of a magnetar and the collision between H-poor

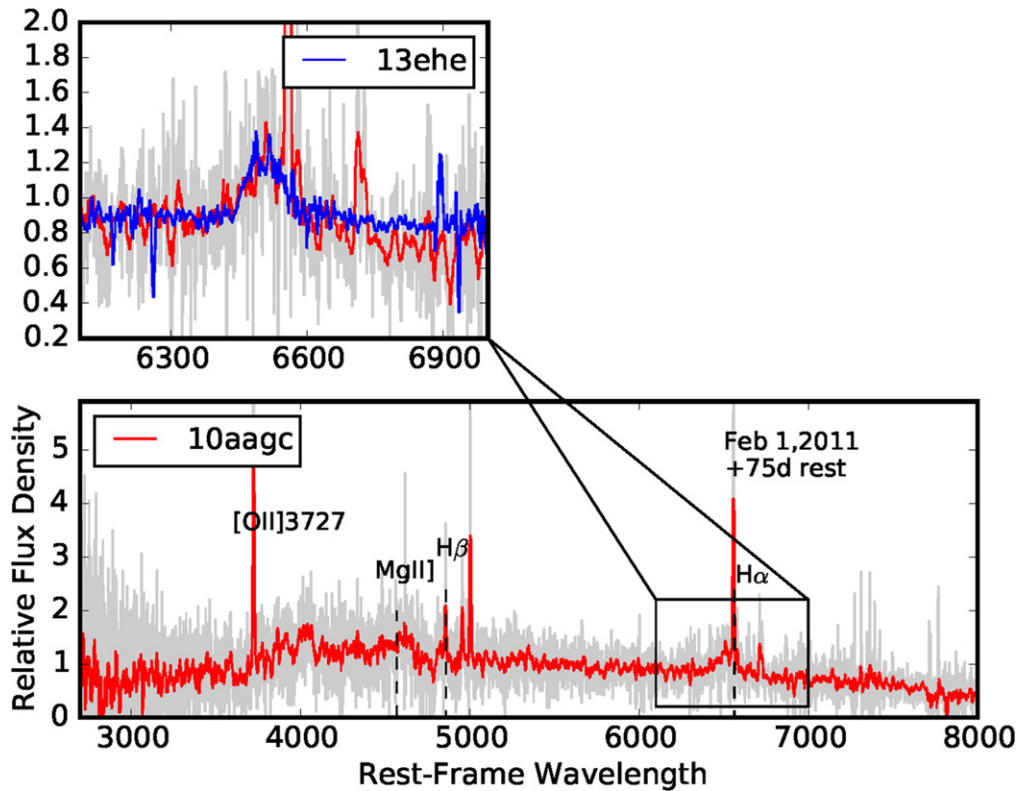


Figure 10. Late-time spectrum of PTF10aagc. We overlaid the smoothed spectrum (red line) on the top of the original data (gray line). The smoothing length is 13 pixels, corresponding to 15 Å. In the zoom-in panel, we compare the broad H α component from iPTF13ehe (blue line) to that from PTF10aagc (red line).

CSM shells. The magnetar scenario clearly needs more scrutiny in the future.

4.4. How Common are the SLSNe-I with Late-time Balmer Emission Lines?

If PPISN is a possible model to explain iPTF13ehe, a related question is how common such an event is among all SLSNe-I. This question is difficult to answer because it depends on when spectroscopic observations are taken. Of the 23 SLSNe-I at $z < 0.4$ PTF discovered during 2009–2013, 13 events have at least 1 spectrum taken after 100 days post-peak. Of these 13 events, we found 2 cases with Balmer emission lines in the late-time spectra. The second case is PTF10aagc, an H-poor SLSN at $z = 0.207$. Figure 10 shows the spectra taken at the phase of +75 days post-peak (rest-frame), revealing a broad H α and the corresponding weak, but detected H β . PTF10aagc may be another case of a SLSN-I with ejecta interaction with a H-rich CSM at late times, although in many ways PTF10aagc is different from iPTF13ehe. Detailed discussion of this object is included in R. M. Quimby et al. (2015, in preparation). Our data suggest that at least 15% of all SLSNe-I have late-time (>100 days post-peak) Balmer emission lines from ejecta interactions with H-rich CSM. It is possible that much higher fractions of SLSNe-I would eventually show late-time spectral signatures of interaction with H-rich CSM. However, the answer must depend on the mass loss mechanism of the SLSN-I progenitor stars.

5. SUMMARY

iPTF13ehe shows the photometric and spectroscopic properties of an SLSN-R, similar to SN2007bi. The key

characteristics are the long rise time (83–148 days) and slow decay rate ($0.0149 \text{ mag day}^{-1}$), different from many SLSNe-I (Quimby et al. 2011). The slow, linear decline of the rest-frame g -band LC does not completely rule out the radioactive decay as a possible power source because we do not have the proper late-time bolometric LC, which is required to make a meaningful comparison with the ^{56}Co decay rate of $0.00977 \text{ mag day}^{-1}$. Another feature that distinguishes iPTF13ehe from most SLSNe-I is its low blackbody temperature at the peak brightness, implying a very large photospheric radius. We measured the peak bolometric luminosity of $1.3 \times 10^{44} \text{ erg s}^{-1}$ and ejecta velocity of $13,000 \text{ km s}^{-1}$. The inferred ejecta mass is very large, in the range of $70\text{--}220 M_{\odot}$, implying a very massive progenitor star regardless of the details of explosion physics. The energetics of iPTF13ehe is in the extreme, with a radiative energy of $\sim 10^{51} \text{ erg}$ and a supernova kinetic energy of $> 10^{53} \text{ erg}$, posing strong challenges to standard core-collapse models. The derived kinetic energy E_{kin} to the ejecta mass M_{ej} ratio in the units of $10^{51} \text{ erg} / 1 M_{\odot}$ is ~ 1.6 .

The new discovery from the iPTF13ehe observations is the detection of a broad H α emission line with a velocity of 4000 km s^{-1} in its nebular-phase spectra taken at 251–278 days. The late-time appearance of H α emission in iPTF13ehe is unique, very different from SN2008es (Gezari et al. 2009; Miller et al. 2009) and CSS121015:004244+132827 (Benetti et al. 2014). For these two superluminous events, although their early-time spectra revealed no traces of hydrogen, the broad H α emission lines were detected after $\sim +40$ days post-peak. It is likely that hydrogen exists in the photosphere, but is probably mostly ionized due to very hot temperature. Only

after +40 days post-peak when the photosphere cools down, the H-recombination lines start to appear.

The situation in iPTF13ehe is quite different. There are no hydrogen features at all in all of the early-time spectra, even when the temperature measured from the spectra is quite cool (7000 K at the peak). A broad and strong H α emission line only emerged in the late-time nebular spectra. Independent of explosion models, this observation reveals the existence of a discrete and distant H-rich shell, which must have been expelled from the progenitor star some years ago before the supernova explosion. The estimated shell mass and the associated kinetic energy of 10^{49} erg s $^{-1}$ suggest that the violent mass loss episodes are extremely energetic, able to unbind the entire hydrogen envelope. One model that predicts such energetic mass losses is PPISN for a star with an initial mass of 95–150 M_{\odot} (Woosley et al. 2007).

The results from iPTF13ehe suggest that future surveys of SLSNe at low redshifts ($z < 0.4$) need to have well-designed plans for the late-time follow-up observations, particularly at the nebular phase. Any attempt to measure the statistics of PPISN candidates like iPTF13ehe would require more systematic follow-up observations than what have been done so far.

We thank the anonymous referee for the positive and constructive suggestions, which have helped to improve the paper. We benefited from discussions with Nick Scoville and Orly Gnat on collisional excitations in ISM. We thank Mansi Kasliwal, Thomas Prince, and Howard Bond for helping us obtain the P200 photometry at one epoch. Vicki Toy and John Capone from University of Maryland are acknowledged for taking the photometry observation using LMI on DCT. A.G.Y. is supported by EU/FP7 via ERC grant No. 307260, the Quantum universe I-Core program by the Israeli Committee for planning and budgeting and the ISF; by Minerva and ISF grants; by the Weizmann-UK “making connections” program; and by Kimmel and ARCHES awards. The Dark Cosmology Centre is funded by the Danish National Research Foundation. This paper made use of Lowell Observatory’s Discovery Channel Telescope (DCT). Lowell operates the DCT in partnership with Boston University, Northern Arizona University, the University of Maryland, and the University of Toledo. Partial support of the DCT was provided by Discovery Communications. The Large Monolithic Imager (LMI) on DCT was built by Lowell Observatory using funds from the National Science Foundation (AST-1005313). LANL participation in iPTF is supported by the US Department of Energy as a part of the Laboratory Directed Research and Development program. A portion of this work was carried out at the Jet Propulsion Laboratory under a Research and Technology Development Grant, under contract with the National Aeronautics and Space Administration. US Government support is acknowledged. This research has made use of the NASA/IPAC Extragalactic Database (NED), which is operated by the Jet Propulsion Laboratory, California Institute of Technology, under contract with the National Aeronautics and Space Administration. Some of the data presented herein were obtained at the W. M. Keck Observatory, which is operated as a scientific partnership among the California Institute of Technology, the University of California, and the National Aeronautics and Space Administration. The Observatory was made possible by the generous

financial support of the W. M. Keck Foundation. The authors wish to recognize and acknowledge the very significant cultural role and reverence that the summit of Mauna Kea has always had within the indigenous Hawaiian community. We are most fortunate to have the opportunity to conduct observations from this mountain.

Facilities: Palomar, Keck, *SWIFT*, Discovery Channel Telescope.

REFERENCES

- Arnett, W. D. 1982, *ApJ*, **253**, 785
- Arnett, D. 1996, *Supernovae and Nucleosynthesis: An Investigation of the History of Matter, from the Big Bang to the Present*, ed. D. Arnett (Princeton, NJ: Princeton Univ. Press), 421
- Barkat, Z., Rakavy, G., & Sack, N. 1967, *PhRvL*, **18**, 379
- Benetti, S., Nicholl, M., Cappellaro, E., et al. 2014, *MNRAS*, **441**, 289
- Bersten, M. C., Benvenuto, O., & Hamuy, M. 2011, *ApJ*, **729**, 61
- Bersten, M. C., Benvenuto, O. G., Nomoto, K., et al. 2012, *ApJ*, **757**, 31
- Bond, J. R., Arnett, W. D., & Carr, B. J. 1984, *ApJ*, **280**, 825
- Branch, D. 2004, in *Cosmic Explosions in Three Dimensions*, ed. P. Hofflich (Cambridge: Cambridge Univ. Press), 132
- Bruzual, G., & Charlot, S. 2003, *MNRAS*, **344**, 1000
- Cardelli, J. A., Clayton, G. C., & Mathis, J. S. 1989, *ApJ*, **345**, 245
- Cenko, S. B., Fox, D. B., moon, D.-S., et al. 2006, *PASP*, **118**, 1396
- Chatzopoulos, E., & Wheeler, J. C. 2012, *ApJ*, **760**, 154
- Chen, T.-W., Smartt, S. J., Jerkstrand, A., et al. 2014, arXiv:1409.7728
- Chevalier, R. A., & Irwin, C. M. 2011, *ApJL*, **729**, L16
- Chevalier, R. A., Kirshner, R. P., & Raymond, J. C. 1980, *ApJ*, **235**, 186
- Davies, B., Figer, D. F., Kudritzki, R.-P., et al. 2009, *ApJ*, **707**, 844
- Drake, A. J., Djorgovski, S. G., Mahabal, A., et al. 2009, *ApJ*, **696**, 870
- Duncan, R. C., & Thompson, C. 1992, *ApJL*, **392**, L9
- Faber, S. M., Phillips, A. C., Kibrick, R. I., et al. 2003, *Proc. SPIE*, **4841**, 1657
- Gal-Yam, A. 2012, *Sci*, **337**, 927
- Gal-Yam, A., Mazzali, P., Ofek, E. O., et al. 2009, *Natur*, **462**, 624
- Gezari, S., Halpern, J. P., Grupe, D., et al. 2009, *ApJ*, **690**, 1313
- Heger, A., & Woosley, S. E. 2002, *ApJ*, **567**, 532
- Heger, A., Woosley, S. E., & Spruit, H. C. 2005, *ApJ*, **626**, 350
- Hogg, D. W., Baldry, I. K., Blanton, M. R., & Eisenstein, D. J. 2002, arXiv:astro-ph/0210394
- Insera, C., Smartt, S. J., Jerkstrand, A., et al. 2013, *ApJ*, **770**, 128
- Kaiser, N., Aussel, H., Burke, B. E., et al. 2002, *Proc. SPIE*, **4836**, 154
- Kasen, D., & Bildsten, L. 2010, *ApJ*, **717**, 245
- Katz, B., Kushnir, D., & Dong, S. 2013, arXiv:1301.6766
- Kennicutt, R. C., Jr. 1998, *ARA&A*, **36**, 189
- Laher, R. R., Surace, J., Grillmair, C. J., et al. 2014, *PASP*, **126**, 674
- Law, N. M., Kulkarni, S. R., Dekany, R. G., et al. 2009, *PASP*, **121**, 1395
- Leoudas, G., Schulze, S., Krühler, T., et al. 2015, *MNRAS*, **449**, 917
- Lunnan, R., Chornock, R., Berger, E., et al. 2014, *ApJ*, **787**, 138
- Masci, F. 2014, http://spider.ipac.caltech.edu/staff/fmasci/home/miscscience/masci_iPTFworkshop2014_ptfide.pdf
- Mazzali, P. A., Deng, J., Nomoto, K., et al. 2006, *Natur*, **442**, 1018
- Mazzali, P. A., Kawabata, K. S., Maeda, K., et al. 2007, *ApJ*, **670**, 592
- Mazzali, P. A., Sauer, D. N., Pastorello, A., Benetti, S., & Hillebrandt, W. 2008, *MNRAS*, **386**, 1897
- Miller, A. A., Chornock, R., Perley, D. A., et al. 2009, *ApJ*, **690**, 1303
- Moriya, T., Tominaga, N., Tanaka, M., Maeda, K., & Nomoto, K. 2010, *ApJL*, **717**, L83
- Moriya, T. J., & Maeda, K. 2014, *ApJL*, **790**, L16
- Morlino, G., Blasi, P., Bandiera, R., & Amato, E. 2013, *A&A*, **558**, A25
- Newman, J. A., Cooper, M. C., Davis, M., et al. 2013, *ApJS*, **208**, 5
- Nicholl, M., Smartt, S. J., Jerkstrand, A., et al. 2013, *Natur*, **502**, 346
- Nicholl, M., Smartt, S. J., Jerkstrand, A., et al. 2015, arXiv:1505.01078
- Ofek, E. O., Arcavi, I., Tal, D., et al. 2014, *ApJ*, **788**, 154
- Ofek, E. O., Cameron, P. B., Kasliwal, M. M., et al. 2007, *ApJL*, **659**, L13
- Oke, J. B., Cohen, J. G., Carr, M., et al. 1995, *PASP*, **107**, 375
- Oke, J. B., & Gunn, J. E. 1983, *ApJ*, **266**, 713
- Padmanabhan, T. (ed.) 2000, *Theoretical Astrophysics*, Vol. 1 (Cambridge: Cambridge Univ. Press), 622
- Pastorello, A., Smartt, S. J., Botticella, M. T., et al. 2010, *ApJL*, **724**, L16
- Planck Collaboration, Ade, P. A. R., Aghanim, N., et al. 2015, arXiv:1502.01589
- Quimby, R. M., Kulkarni, S. R., Kasliwal, M. M., et al. 2011, *Natur*, **474**, 487

- Rahmer, G., Smith, R., Velur, V., et al. 2008, *Proc. SPIE*, 7014, 70144Y
- Rakavy, G., & Shaviv, G. 1967, *ApJ*, 148, 803
- Rau, A., Kulkarni, S. R., Law, N. M., et al. 2009, *PASP*, 121, 1334
- Scannapieco, E., Madau, P., Woosley, S., Heger, A., & Ferrara, A. 2005, *ApJ*, 633, 1031
- Schlafly, E.F., & Finkbeiner, D. P. 2011, *ApJ*, 737, 103
- Smith, N., Li, W., Foley, R. J., et al. 2007, *ApJ*, 666, 1116
- Smith, N., & McCray, R. 2007, *ApJL*, 671, L17
- Sorokina, E., Blinnikov, S., Nomoto, K., Quimby, R., & Tolstov, A. 2015, arXiv:1510.00834
- Waldman, R. 2008, *ApJ*, 685, 1103
- Woosley, S. E. 2010, *ApJL*, 719, L204
- Woosley, S. E., Blinnikov, S., & Heger, A. 2007, *Natur*, 450, 390
- Yaron, O., & Gal-Yam, A. 2012, *PASP*, 124, 668
- Yoon, S.-C., Dierks, A., & Langer, N. 2012, *A&A*, 542, A113
- Young, D. R., Smartt, S. J., Valenti, S., et al. 2010, *A&A*, 512, A70